LRP 570/97 March 1997

GLOBAL APPROACH TO THE SPECTRAL PROBLEM OF MICROINSTABILITIES IN A CYLINDRICAL PLASMA USING A GYROKINETIC MODEL

S. Brunner and J. Vaclavik

Submitted for publication
in Physics of Plasmas

Global Approach to the Spectral Problem of Microinstabilities in a Cylindrical Plasma using a Gyrokinetic Model.

S.Brunner* and J. Vaclavik

Centre de Recherches en Physique des Plasmas, Association Euratom-Confédération Suisse,

Ecole Polytechnique Fédérale de Lausanne, CRPP-PPB, CH-1015 Lausanne, Switzerland

(March 17, 1997)

Abstract

Considering the spectral problem of microinstabilities in a curved system, methods for solving the global gyrokinetic equation are presented for the simple case of a cylindrical plasma. They prove to be efficient for computing the full unstable spectrum of ITG-type modes and have shown to be applicable to the two-dimensional integral equation of tokamak configurations.

52.35.Kt, 52.25.Fi, 52.25.Dg, 52.35.-g

*E-mail: brunner@crppsun.epfl.ch

I. INTRODUCTION.

For studying microinstabilities in tokamak-like plasmas, most linear kinetic studies were carried out for high toroidal wave numbers using the ballooning representation [1]- [6] which leads to a one-dimensional integral equation along the magnetic field lines. Except for very few cases, these calculations do not include a higher order WKB procedure for determining the radial structure. Thus these results usually stay local to a magnetic surface and there remains some questioning on the actual radial extent of these modes. For low toroidal wave numbers where the ballooning representation breaks down and the full two-dimensional problem cannot be reduced, very little linear computation has been carried out. This limit is of interest as it describes larger wavelength fluctuations which could lead to higher turbulent transport. So even at the present state where non-linear simulations already exist [7] [8], there remains a need for global linear studies.

Until recently, the only published results from true global, toroidal, linear computations were based on the spectral code by Marchand, Tang and Rewoldt [9] [10], which is valid to second order in the banana width and contains no finite Larmor radius (FLR) effects. We have therefore undertaken the development of a new global spectral code with the goal of keeping these effects to all orders. This leads to a two-dimensional integral equation which requires appropriate modeling and numerical methods to be solved. Although such toroidal results have already been obtained and benchmarked with a global linear time evolution (particle in cell) code being developed simultaneously [13], we shall present here the methods employed in the case of a simple cylindrical configuration. This system can be considered as the limiting case of a stretched tokamak to a periodic cylindrical plasma with remaining magnetic shear and realistic density and temperature profiles. A following paper will discuss the toroidal model.

Kinetic equations have been solved in the past for spectral problems in cylindrical plasmas when studying mirror-like configurations confined by straight magnetic fields [11] [12]. Fourier representation appears naturally in gyrokinetic theory as it allows one to integrate

A. The Gyrokinetic Equation in Cylindrical Variables.

In fusion plasmas, the ion Larmor radius λ_L is generally small compared with the characteristic length a of equilibrium, one can therefore define the small parameter

$$\epsilon = \lambda_L / a \ll 1. \tag{1}$$

Furthermore, when studying microinstabilities, one can assume gyro-ordering:

$$k_\perp \lambda_L \sim \epsilon^0, \tag{2}$$

$$\frac{k_\parallel}{k_\perp} \sim \epsilon^1, \tag{3}$$

$$\frac{\omega}{\Omega} \sim \epsilon^1, \tag{4}$$

where $(\omega, \vec{k})$ is a typical frequency-wave vector pair of perturbation and Ω the ion cyclotron frequency. In this frame it is appropriate to describe the evolution of the ion distribution function by the linearized gyrokinetic equation (GKE) [15] valid to order $O(\epsilon)$:

$$\left.\frac{D}{Dt}\right|_{u.t.g.} \tilde{g} = \left(\frac{\partial}{\partial t} + \vec{v}_g \cdot \frac{\partial}{\partial \vec{R}}\right) \tilde{g} = \frac{e}{T_i} F_M \frac{\partial < \phi >}{\partial t} + \frac{1}{B} \frac{dF_M}{d\rho} \vec{e}_\theta \cdot \nabla < \phi >, \tag{5}$$

where $\tilde{g} = \tilde{f} + e\phi F_M / T_i$ is the non-adiabatic part of the distribution function $\tilde{f}$, $< \phi >$ the gyroaveraged potential, and F_M the local Maxwellian distribution function with temperature $T_i = T_i(\rho)$ and density $N = N(\rho)$:

$$F_M(\rho, E) = \frac{N}{(2\pi T_i / m_i)^{3/2}} \exp - \left(\frac{E}{T_i / m_i}\right).$$

Eq.(5) is written in gyrokinetic variables $(\vec{R}, E, \mu, \alpha, \mathrm{sign}(v_\parallel))$, with $\vec{R} = \vec{r} + \vec{v} \times \vec{e}_\parallel / \Omega$ the guiding center (GC), $E = \frac{1}{2} v^2$ the kinetic energy, $\mu = \frac{1}{2} v_\perp^2 / B$ the magnetic moment, and α the gyroangle. Although one solves for the particle distribution function, the GKE has taken full advantage of guiding center theory as $\left.\frac{D}{Dt}\right|_{u.t.g.}$ stands for the total time derivative along the unperturbed trajectories of the GC. The GC velocity

$$\vec{v}_g = v_\parallel \vec{e}_\parallel + \vec{v}_d,$$

is divided into parallel motion and drifts:

$$\vec{v}_d = \frac{1}{\Omega}\left[\frac{v_\perp^2}{2} + v_\parallel^2\right] \vec{e}_\parallel \times \nabla \ln B.$$

To be able to perform explicitly the gyroaveraging of the unknown potential, a plane wave decomposition is usually considered:

$$\phi(\vec{r}) = \int d\vec{k}\; e^{i\vec{k}\cdot\vec{r}}\; \hat{\phi}\,(\vec{k}). \tag{6}$$

Gyroaveraging can then be performed analytically with no further approximation:

$$\begin{aligned} <\phi> &= \int d\vec{k}\; e^{i\vec{k}\cdot\vec{R}}\; \hat{\phi}\,(\vec{k}) \frac{1}{2\pi}\int_0^{2\pi} d\alpha\; \exp(-i\;\vec{k}\cdot\frac{\vec{v}\times\vec{e}_\parallel}{\Omega}) \\ &= \int d\vec{k}\; J_0\left(\frac{k_\perp v_\perp}{\Omega}\right) e^{i\vec{k}\cdot\vec{R}}\; \hat{\phi}\,(\vec{k}), \end{aligned}$$

using the integral representation of the Bessel function [16]. Thus Fourier space appears as the natural representation for gyrokinetic theory.

Going back to particle variables $(\vec{r}, \vec{v})$ and keeping lowest order terms in ϵ, one must essentially replace the factor $\exp i\;\vec{k}\cdot\vec{R}$ by $\exp i\;\vec{k}\cdot(\vec{r} + \vec{v}\times\vec{e}_\parallel/\Omega)$ so that

$$\begin{aligned} &\left(\frac{\partial}{\partial t} + \vec{v}_g\cdot\frac{\partial}{\partial\vec{r}}\right)\tilde{g}\,(\vec{r},\vec{v},t) = \\ &\left[\frac{e}{T_i}F_M\frac{\partial}{\partial t} + \frac{dF_M}{d\rho}\frac{1}{B}\,\vec{e}_\theta\cdot\nabla\right]\int d\vec{k}\; J_0\left(\frac{k_\perp v_\perp}{\Omega}\right) e^{i\vec{k}\cdot\vec{r}}\exp(i\;\vec{k}\cdot\frac{\vec{v}\times\vec{e}_\parallel}{\Omega})\;\hat{\phi}\,(\vec{k},t). \end{aligned} \tag{7}$$

For a curved system, the plane wave decomposition (6), although exact [11] [12], leads to relations that do not allow the simple numerical methods presented in Sec.III. For comparison, these relations are established in the Appendix. Instead let us consider another Fourier representation which will be referred to as the cylindrical wave decomposition, so that in the above relations the following terms must be replaced by the corresponding right hand side:

$$\int d\;\vec{k}\; e^{i\vec{k}\cdot\vec{r}}\;\hat{\phi}\,(\vec{k}) \longrightarrow \sum_{m,n}\int d\kappa\;\hat{\phi}_{m,n}\,(\kappa)\exp i(\kappa\rho + m\theta + n\frac{z}{R}).$$

In particular one must reconsider:

$$\vec{k}\cdot\vec{R} = \vec{k}\cdot\vec{r} + \vec{k}\cdot\frac{\vec{v}\times\vec{e}_{\|}}{\Omega} \tag{8}$$
$$\longrightarrow \left(\kappa\rho + m\theta + n\frac{z}{R}\right) + \left(\kappa\nabla\rho + m\nabla\theta + \frac{n}{R}\nabla z\right)\cdot\frac{\vec{v}\times\vec{e}_{\|}}{\Omega} + O(\epsilon^2).$$

Note that the last relation is valid only to order $O(\epsilon)$. The effect of this approximation will be discussed further on. From Eq.(8) the local wave vector can be deduced

$$\vec{k}\longrightarrow \kappa\nabla\rho + m\nabla\theta + \frac{n}{R}\nabla z = \kappa\,\vec{e}_\rho + \frac{m}{\rho}\,\vec{e}_\theta + \frac{n}{R}\,\vec{e}_z\,.$$

As the system is homogeneous along θ, z and time, the poloidal and toroidal wave numbers (m, n) can be fixed, as well as the frequency ω:

$$\phi(\vec{r},t) = \phi(\rho)\exp i(m\theta + n\frac{z}{R} - \omega t). \tag{9}$$

Thus, the linear study becomes an effectively one dimensional problem along the radial direction.

One can easily show that $\vec{e}_\rho\cdot\vec{v}_d = 0$ so that the GC trajectories lie on magnetic surfaces ρ =const. This leads to a trivial solving of the gyrokinetic equation:

$$\tilde{f}\,(\rho,\vec{v}) = \frac{e}{T_i}\left[-\phi(\rho)F_M + \frac{(\omega-\omega^\star)F_M}{\omega - k_{\|}v_{\|} - \omega_g}\int d\kappa J_0(\frac{k_\perp v_\perp}{\Omega})e^{i\kappa\rho}\exp(i\,\vec{k}\cdot\frac{\vec{v}\times\vec{e}_{\|}}{\Omega})\,\hat{\phi}\,(\kappa)\right], \tag{10}$$

with $k_{\|} = (nq_s - m)/Rq_s$, $k_\theta = m/\rho$, $k_\perp = \sqrt{\kappa^2 + k_\theta^2}$, the different components of the wave vector, and

$$\omega_g = k_\theta v_d = -\frac{1}{\Omega}\left(\frac{v_\perp^2}{2} + v_{\|}^2\right)\frac{k_\theta}{R_\theta}, \qquad \frac{1}{R_\theta} = \frac{1}{Rq_s}\frac{d}{d\rho}\left(\frac{\rho^2}{Rq_s}\right),$$
$$\omega^\star = \omega_n\left(1 + \eta T_i\frac{\partial}{\partial T_i}\right), \qquad \omega_n = \frac{T_i}{eB}\frac{d\ln N}{d\rho}k_\theta,$$

the guiding center and diamagnetic drift frequencies, $\eta = d\ln T_i/d\ln N$. In (10) $\Im m(\omega)$ is taken positive to ensure causality.

B. The Eigenvalue Equation.

For the low frequency microinstabilities, the system can be closed invoking quasineutrality:

$$\varrho_q^{int} = e(n_i - n_e) \simeq 0, \tag{11}$$

n_i and n_e being respectively the ion and electron densities. This relation must hold as well for the stationary state as for the fluctuating parts. Hence, the perturbed ion density $\tilde{n}_i$ is evaluated:

$$\tilde{n}_i(\rho) = \int \tilde{f}(\rho, \vec{v}) d\vec{v} =$$
$$\frac{Ne}{T_i}\left[-\phi(\rho) + (\omega - \omega^*)\int d\kappa e^{i\kappa\rho}\,\hat{\phi}(\kappa)\frac{1}{(2\pi v_{thi}^2)^{3/2}}\int d\vec{v}\,\frac{J_0^2(k_\perp v_\perp/\Omega_i)\exp(-v^2/2v_{thi}^2)}{\omega - k_{||}v_{||} - \omega_g}\right],$$

where $d\vec{v} = 2\pi v_\perp dv_\perp dv_{||}$, the integral over α having again been performed analytically. For studying ITG instabilities, the perturbed electron density may be reduced to the adiabatic response:

$$\tilde{n}_e = \frac{e\phi}{T_e}N.$$

Inverting the Fourier representation by expressing $\hat{\phi}(\kappa)$ in terms of $\phi(\rho)$, the quasineutrality equation now becomes :

$$-\varrho_q^{int}(\rho) = \int d\rho' \mathcal{K}(\rho, \rho'; \omega)\phi(\rho') = 0, \tag{12}$$

with

$$\mathcal{K}(\rho, \rho'; \omega) = \frac{Ne^2}{T_i}\left[\left(\frac{1}{\tau} + 1\right)\delta(\rho - \rho') - \mathcal{N}(\rho, \rho'; \omega)\right], \tag{13}$$

$$\mathcal{N}(\rho, \rho'; \omega) = \frac{1}{2\pi}\int d\kappa \exp(i\kappa|\rho - \rho'|)\,\hat{\mathcal{N}}(\rho, \kappa; \omega), \tag{14}$$

$$\hat{\mathcal{N}}(\rho, \kappa; \omega) = (\omega - \omega^*)\frac{1}{(2\pi v_{thi}^2)^{3/2}}\int d\vec{v}\,\frac{J_0^2(k_\perp v_\perp/\Omega)\exp(-v^2/2v_{thi}^2)}{\omega - k_{||}v_{||} - \omega_g}, \tag{15}$$

all equilibrium quantities being evaluated at ρ and having defined $\tau = T_e/T_i$. Eq(12) is an eigenvalue equation, i.e. one must find the complex frequencies ω for which there exists a non trivial function ϕ verifying this relation.

In a first approximation, GC drifts are neglected in the resonant denominator so that the velocity integrals can be separated and expressed in terms of the scaled modified Bessel function $\Lambda_p(x) = e^{-x}I_p(x)$ and the plasma dispersion function $W(z)$ [17]:

$$\frac{1}{(2\pi v_{thi}^2)^{3/2}} \int d\vec{v}\, \frac{J_0^2(k_\perp v_\perp/\Omega)\exp(-v^2/2v_{thi}^2)}{\omega - k_{||}v_{||}} = -\Lambda_0(\xi)\frac{1}{\omega}\left[W(z)-1\right], \tag{16}$$

with the definitions $\xi = (k_\perp \lambda_L)^2$, $\lambda_L = v_{thi}/\Omega$, $z = \omega/|k_{||}|v_{thi}$ and

$$W(z) = \frac{1}{\sqrt{2\pi}} \int_{-\infty}^{+\infty} \frac{x}{x-z} \exp(-\frac{x^2}{2}) dx \quad , \quad \Im m(z) > 0.$$

When carrying out the derivative with respect to T_i:

$$\begin{aligned} \hat{\mathcal{N}}(\rho,\kappa;\omega) &= \left(\frac{\omega^\star}{\omega} - 1\right)(W-1)\Lambda_0 \qquad (17)\\ &= \left[\frac{\omega_n}{\omega}\left(1-\frac{\eta}{2}\right) - 1\right](W-1)\Lambda_0 + \frac{\omega_n}{\omega}\eta\left[\frac{z^2}{2}W\Lambda_0 + (W-1)\xi(\Lambda_1 - \Lambda_0)\right], \end{aligned}$$

using the notations $W = W(z)$, $\Lambda_p = \Lambda_p(\xi)$. The integral representation for the modified Bessel function [16]

$$I_p(x) = \frac{1}{\pi}\int_0^\pi e^{x\cos\nu}\cos(p\nu)d\nu,$$

allows one to replace the integral over the infinite domain of κ appearing in $\mathcal{N}$ by the integral over the finite interval of the new variable ν [18]:

$$\begin{aligned} \mathcal{N}(\rho,\rho';\omega) &= \left(\frac{\omega^\star}{\omega} - 1\right)(W-1)\frac{1}{2\pi\lambda_L}\int_0^\pi \frac{d\nu}{\sqrt{\pi(1-\cos\nu)}} \times \\ &\exp - \left[\left(\frac{m\lambda_L}{\rho}\right)^2 (1-\cos\nu) + \left(\frac{\rho-\rho'}{2\lambda_L}\right)^2 \frac{1}{1-cos\nu}\right], \qquad (18) \end{aligned}$$

This last step will be useful when performing numerical integration.

C. Properties of the integral equation.

1. Local dispersion relation.

The eigenvalue problem is formulated as a one-dimensional integral equation for the radial dependence of the electrostatic potential. Notice that the only radial coupling comes from finite Larmor radius (FLR) effects appearing in (17) through the argument ξ and explicitly brought forth in relation (18). By taking $\xi = (k_\theta \lambda_L)^2$ one neglects this coupling and finds a local dispersion relation for each magnetic surface:

lowest order in ϵ. Let us write all equilibrium terms depending on the variable ρ as in the following case for temperature :

$$T(\rho) = T\left(\frac{\rho+\rho'}{2}\right) + \frac{\rho-\rho'}{2}\frac{dT}{d\rho} + \ldots = T\left(\frac{\rho+\rho'}{2}\right) + O(\epsilon),$$

where we have used the fact that the radial coupling distance is of the order of the Larmor radius ($|\rho - \rho'| \sim \lambda_L$). In this way and to order to which we work, one can verify (22).

3. Boundary conditions.

As the equation is of integral type, it already contains boundary conditions. Expressions (12), (13) and (18) evidently show that the regularity condition at $\rho = 0$

$$\phi_m(\rho = 0) = 0 \quad \text{if} \quad m \neq 0, \tag{23}$$

is verified. However, we will see in the next point that the full regularity condition expected:

$$\phi_m(\rho) \sim \rho^{|m|} \quad \text{as} \quad \rho \longrightarrow 0, \tag{24}$$

is not exactly fulfilled. At the edge of the plasma, where the electron temperature falls to zero, one has the boundary condition

$$\phi_m(\rho = a) = 0, \tag{25}$$

for all values of m.

4. Fluid limit

To get a better understanding of the behavior of Eq.(12) on the axis, the limiting case of cold ions is considered, so that the integral equation becomes differential:

$$\left\{\omega^2\left[1 - \lambda_L^{\star 2}\left(\frac{d^2}{d\rho^2} - \frac{m^2}{\rho^2}\right)\right] - \omega\omega_{ne} - k_{||}^2 c_s^2\right\}\phi = 0, \tag{26}$$

with $c_s^2 = T_e/m_i$, $\lambda_L^\star = c_s/\Omega$ and $\omega_{ne} = -\tau\omega_n$. Note that the only radial coupling, i.e. the differential character of the equation, comes from the polarization drift, which is the remaining FLR effect in the cold limit.

The question is whether Eq.(26) still contains approximations related to gyro-ordering. Had one intended to derive this relation from the basic set of fluid equations, that is the linearized equation of motion for cold magnetized ions:

$$m_i \frac{\partial \vec{v}}{\partial t} = e\left(\vec{v} \times \vec{B} - \nabla\phi\right),$$

the equation of continuity, the Boltzmann equation for electrons and invoking again quasineutrality, would have obtained [20]:

$$\left\{\omega^2\left[1 - \lambda_L^{\star 2}\left(\frac{1}{\rho}\frac{d}{d\rho}\rho\frac{d}{d\rho} - \frac{m^2}{\rho^2}\right)\right] - \omega\omega_{ne} - k_\parallel^2 c_s^2\right\}\phi = 0. \tag{27}$$

Note the difference with Eq.(26). This can be traced back to the approximation in relation (8) where the factor $1/|\nabla\theta| = \rho$, corresponding to the Jacobian in cylindrical variables, was treated as a characteristic length of equilibrium. As a consequence, this approximation leads to the following behavior on the axis

$$\phi_m(\rho) \sim \rho^{m'} \quad , \quad m' = \frac{1 + \sqrt{1 + 4m^2}}{2}, \tag{28}$$

instead of (24). However, for large values of $|m|$ this difference becomes negligible.

By considering Eqs(44)- (46) of the Appendix obtained with the plane wave decomposition, which are exact in this respect, and applying the asymptotic relation for the modified Bessel function

$$\Lambda_m(x) \longrightarrow \frac{1}{\sqrt{2\pi x}} \exp -\frac{m^2}{2x} \quad \text{as} \quad x \longrightarrow \infty,$$

which also improves for low arguments with increasing mode number m, one recovers Eqs (12), (13) and (18). Therefore, a few Larmor radii off the axis or for not too small poloidal mode numbers, the discussed difference is negligible. This is the case in practice where the linear instabilities are localized around the region of steepest gradients, i.e. usually around

mid-point between the magnetic axis and plasma edge. Furthermore, for ITG instabilities $k_{\|} \simeq 0$, so that $m \simeq nq_s \neq 0$ if the toroidal mode number n is non zero. Finally Eq.(43) shows that in cylindrical geometry the plane wave decomposition actually leads to a Bessel representation instead of the handier Fourier transform appearing in (14). This illustrates how in a more complex geometry the plane wave decomposition simply becomes intractable.

III. NUMERICAL METHOD

The eigenvalue equation must be approximated by a finite set of simultaneous algebraic linear equations. In a first approach one solves the equation for the potential $\phi = \phi(\rho)$ in configuration space, as given by Eq.(12). In a second approach the equation for the potential written in Fourier representation $\hat{\phi}=\hat{\phi}(\kappa)$ is solved. Although the first technique cannot be directly generalized to a toroidal system due to the significantly more complicated particle trajectories, it is a useful benchmark here for testing whether the Fourier method is appropriate for a finite system.

A. Solving in configuration space

Equation (12) is classified as a linear homogeneous Fredholm equation of the second kind. As can be seen in relation (18), its kernel $\mathcal{N}(\rho, \rho'; \omega)$ exhibits a singularity at $\rho = \rho'$ with a characteristic length of the order of the ion Larmor radius. This is obviously related to the radial coupling due to FLR effects. Integrating this singularity numerically over ρ' would require a sufficient number of integration points in an interval of order λ_L. However, by using a finite element method, this can actually be performed analytically. Let us approximate $\phi(\rho)$ using a set of linearly independent basis functions $\{\gamma_i(\rho)\}_{i=1,\ldots,n_r}$:

$$\phi(\rho) = \sum_{i=1}^{n_r} \phi_i \gamma_i(\rho). \tag{29}$$

For the purpose of solving the integral equation, it is sufficient to take constant elements:

$$I_{ij} = \frac{1}{\lambda_L^2(1-\cos\nu)} \int_{\rho_{i-1}}^{\rho_i} d\rho \int_{\rho_{j-1}}^{\rho_j} d\rho' \exp\left[-\left(\frac{\rho-\rho'}{2\lambda_L}\right)^2 \frac{1}{1-\cos\nu}\right]$$
$$= -2\left[\sqrt{\pi} x_{ij}\,\mathrm{erf}(x_{ij}) + e^{-x_{ij}^2}\right]\Big|_{i-1}^{i}\Big|_{j-1}^{j},$$

where $x_{ij} = (\rho_i - \rho_j)/(2\lambda_L\sqrt{1-\cos\nu})$ and $\mathrm{erf}(z) = (2/\sqrt{\pi})\int_0^z e^{-t^2}dt$ is the error function. Finally, performing the derivative with respect to temperature contained in $\omega^\star$ gives

$$M_{ij} = \frac{Ne^2}{T_{ion}}\bar{\rho}_i\left[\left(\frac{1}{\tau}+1\right)\Delta\rho_i\,\delta_{ij}\right.$$
$$\left. -\left\{\left[\frac{\omega_n}{\omega}\left(1-\frac{\eta}{2}\right)-1\right](W-1) + \frac{\omega_n}{\omega}\eta\frac{z^2}{2}W\right\}C_{ij} - \frac{\omega_n}{\omega}\eta(W-1)C'_{ij}\right], \tag{32}$$

$$C_{ij} = \frac{\lambda_L}{2\pi}\int_0^\pi d\nu\sqrt{\frac{1-\cos\nu}{\pi}}\exp\left[-(m\lambda_L/\bar{\rho}_i)^2(1-\cos\nu)\right] I_{ij}, \tag{33}$$

$$C'_{ij} = T_{ion}\frac{\partial}{\partial T_{ion}}C_{ij} = -\frac{\lambda_L}{2\pi}\int_0^\pi d\nu\sqrt{\frac{1-\cos\nu}{\pi}}\times \tag{34}$$
$$\exp\left[-\left(\frac{m\lambda_L}{\bar{\rho}_i}\right)^2(1-\cos\nu)\right]\left[\left(\frac{m\lambda_L}{\bar{\rho}_i}\right)^2(1-\cos\nu)I_{ij} + e^{-x_{ij}^2}\Big|_{i-1}^{i}\Big|_{j-1}^{j}\right].$$

The integrals over ν in the definitions of the coupling matrices C_{ij} and C'_{ij} were computed using an extended trapezoidal rule. These matrices are sparse band as two elements γ_i and γ_j are coupled only if they are contained in the same interval of a few Larmor radii. The significant off-diagonal terms are therefore such that

$$C_{ij}, C'_{ij} \neq 0 \quad \Longleftrightarrow \quad \left|\bar{\rho}_i - \bar{\rho}_j\right| \lesssim l\lambda_L,$$

where typically $l \simeq 8$. In addition, note that these matrices are independent of ω and can therefore be precalculated.

The analytic continuation of the dispersion function to the whole complex plane can be expressed as

$$W(z) = 1 + i\sqrt{\frac{\pi}{2}}z\,e^{-z^2}\left[1+\mathrm{erf}(iz)\right],$$

where the complex error function can be computed efficiently using an algorithm by W.Gautschi [21].

B. Solving in Fourier space

By performing a Fourier transform of Eq.(12), one obtains an equivalent equation for $\hat{\phi}(\kappa)$. Because the radial domain is finite, one can actually perform a Fourier series instead of a Fourier transform. This alternative is of interest as the equation then becomes naturally discrete with no singularity to be integrated:

$$\sum_{k'=-\infty}^{+\infty} \hat{M}_{kk'}(\omega)\,\hat{\phi}_{k'} = \sum_{k'=-\infty}^{+\infty} \hat{\mathcal{K}}_{k-k',k'}(\omega)\,\hat{\phi}_{k'} = 0, \tag{35}$$

$$\phi(\rho) = \sum_{k=-\infty}^{+\infty} \hat{\phi}_k \exp i\frac{2\pi}{\Delta\rho}k(\rho-\rho_0), \tag{36}$$

$$\hat{\mathcal{K}}_{k'',k'}(\omega) = \frac{1}{\Delta\rho}\int_{\rho_0}^{\rho_{n_r}} d\rho \frac{Ne^2}{T_i}\left[\frac{1}{\tau}+1-\hat{\mathcal{N}}\left(\rho,\kappa'=k'\frac{2\pi}{\Delta\rho};\omega\right)\right]\exp -i\frac{2\pi}{\Delta\rho}k''(\rho-\rho_0),$$

where $\Delta\rho=\rho_{n_r}-\rho_0$ is the width of the considered radial interval. To compute the elements $\hat{\mathcal{K}}_{k''k'}(\omega)$, an equidistant mesh $\{\rho_i\}_{i=0,\ldots,n_r}$ was taken so that fast Fourier transform algorithms could be applied. This gives rise to n_r non-zero elements $\hat{\mathcal{K}}_{k''k'}$, $-n_r/2 \tilde{<} k'' \tilde{<} n_r/2$, i.e. $\hat{M}$ is a band matrix with $\sim n_r/2$ sub- and super-diagonals. As opposed to the required mesh density when solving in configuration space, note that here the radial mesh need only resolve equilibrium quantities. Therefore, the number of off-diagonals in $\hat{M}$ increases with the inhomogeneity of equilibrium. However, the sums over k and k' in Eq.(35) and (36) related to the Fourier series of the perturbing electrostatic potential are truncated at $\pm k_{max}$ such that

$$k_{max}\frac{2\pi}{\Delta\rho}\lambda_L \sim 1,$$

in agreement with gyro-ordering.

When solving over the whole radial interval $[0,a]$, note that the boundary conditions (23) and (25) still are contained in Eq.(35) but in Fourier representation now read

$$\lim_{\rho\to 0}\sum_k \hat{\phi}_k\, e^{ik\frac{2\pi}{a}\rho} = 0, \quad \text{if} \quad m\neq 0,$$

$$\lim_{\rho\to a}\sum_k \hat{\phi}_k\, e^{ik\frac{2\pi}{a}\rho} = 0.$$

Unlike the approach in configuration space, no assumption has yet been made concerning drifts. Although this requires two additional velocity integrals, and for typical physical values leads only to minor corrections of ITG-instabilities, drifts can be considered here with no further difficulty. Keeping these terms and defining the dimensionless velocity variable $\vec{\mathsf{v}}=\vec{v}\ /v_{thi}$, Eq.(35) has to be solved with $\hat{\mathcal{N}}$ given by:

$$\hat{\mathcal{N}}\left(\rho,\kappa;\omega\right)=\int_0^{+\infty}d\mathsf{v}_\perp\mathsf{v}_\perp J_0^2\left(\sqrt{\kappa^2+k_\theta^2}\lambda_L\mathsf{v}_\perp\right)e^{-\mathsf{v}_\perp^2}\times$$
$$\frac{1}{\sqrt{2\pi}}\int_{-\infty}^{+\infty}d\mathsf{v}_{||}\frac{z-\frac{\omega_n}{|k_{||}|v_{thi}}\left[1+\frac{\eta}{2}\left(\mathsf{v}_{||}^2+\mathsf{v}_\perp^2-3\right)\right]}{z-\mathsf{v}_{||}-\omega_g(\mathsf{v}_{||},\mathsf{v}_\perp)/|k_{||}|v_{thi}}e^{-\mathsf{v}_{||}^2}. \tag{37}$$

The Gaussian velocity distribution allows one to approximate the integration boundaries at $\pm\infty$ by finite values $\pm\mathsf{v}_{max||,\perp}\sim 5$. Extended trapezoidal rules are applied for these numerical quadratures. One must still point out that unless performing an integration along a contour in the complex $\mathsf{v}_{||}$ plane, so as to avoid, in agreement with causality, the poles related to the resonant denominator, relation (37) is only valid for frequencies such that $\Im m(\omega)>0$. This is assumed here, as it greatly simplifies the velocity integration, however it restricts the study to unstable modes.

C. Searching for the eigenfrequencies.

Once the eigenvalue equation has been cast in one of the matrix forms (30) or (35), the problem of finding the eigenfrequencies can be written:

$$D(\omega)=det\,M(\omega)=0. \tag{38}$$

Taking advantage of the fact that $D(\omega)$ is analytic, a practical method proposed by Davies [14] was applied for solving (38). Suppose $h(z)$ is an analytic function inside a closed positively oriented contour C. Having determined the number N of enclosed zeros $\{a_i\}_{i=1,\ldots,N}$ using the principle of argument, the method is then based on the evaluation of an equivalent number of integrals:

$$S_n=\frac{1}{2\pi i}\int_C z^n\frac{h'(z)}{h(z)}dz \qquad n=1,\ldots,N, \tag{39}$$

which have the property

$$S_n = \sum_{i=1}^{N} a_i^n \qquad n = 1, \ldots, N. \tag{40}$$

The set of equations (40) is then solved finding the roots of the associated polynomial defined by

$$P_N(z) = \prod_{i=1}^{N}(z - a_i) = \sum_{i=0}^{N} A_i z^{N-i}. \tag{41}$$

A recursive relation enables to calculate the coefficients A_n from S_n:

$$S_1 + A_1 = 0$$

$$S_2 + A_1 S_1 + 2A_2 = 0$$

$$S_k + A_1 S_{k-1} + A_2 S_{k-2} + \ldots + kA_k = 0 \quad k = 1, \ldots, N.$$

The numerical technique by Davies is developed for circular contours. We have generalized this algorithm to allow for more elongated curves in the frequency plane. This is achieved by applying the above method along a unitary circle to the function $D(z) = D(\omega(z))$ with $\omega(z)$ being a conformal transformation of the unit disc at origin. We chose

$$\omega(z) = \tilde{\omega} + r\, z(Ez^2 + 1), \tag{42}$$

transforming the unit circle in the z-plane to a more oval-shaped curve in the ω-plane centered at $\tilde{\omega}$ with average radius r. The elongation and orientation are defined by the complex parameter E ($|E| \tilde{<} 0.1$).

The sampling points along the contour are increased until the maximum jump in the argument of $D(\omega(z))$ is less then $\pi/2$. Accuracy is usually given with more than four significant digits and allows one to consider up to ten roots inside a single curve.

Having identified an eigenfrequency ω_i, the corresponding eigenmode is computed by considering an inhomogeneous right hand side in (30) or (35) with $\omega = \omega_i$ then solving for ϕ. The initial right hand side is chosen as a first guess of the eigenvector structure. This process is then repeated iteratively until convergence is attained. This approach is inspired by the inverse iterative method for solving standard eigenvalue problems.

Let us still point out that when considering FLR effects to all orders, i.e. solving the integral equation, the spectrum contains no spurious modes.

IV. RESULTS

As an illustration, a hydrogen plasma with the following parameters is considered: major radius $R = 1.\text{m}$, minor radius $a = 0.2\text{m}$, magnetic field on axis $B_0 = 2.\text{Tesla}$, safety factor profile $q_s(s) = 1 + 2s^2$, density profile $N(s)/N_0 = 1 - s^2$, electron temperature profile $T_e(s)/T_{e0} = (1 - s^2)^2$, ion temperature profile $T_i(s)/T_{i0} = (1 - s^2)^3$, temperatures on axis $T_{e0} = T_{i0} = 2.\text{keV}$. Here $s = \rho/a$ stands for the normalized radial variable. The average ion Larmor radius is $\lambda_L \tilde{=} 1.5\,10^{-3}\text{m}$ so that $\epsilon = \lambda_L/a \tilde{=} 7.5\,10^{-3}$. In the frame of our model, the plasma can exhibit slab-like ITG instabilities. For fixed mode numbers (m, n) the plasma is locally unstable if $\eta > \eta_c \tilde{=} 1$ around the mode rational surface, i.e. where $|k_{\|}/k_\theta| \tilde{<} \lambda_L/L_T$, $L_T = |d \ln T_i/d\rho|^{-1}$ being the characteristic length of temperature [19]. Thus the plasma considered here is unstable at any mode rational surface as $\eta(s) \equiv 3$.

Fig.1 shows the unstable spectrum in the complex frequency plane for mode numbers $(m = 8, n = 5)$. All frequencies are normalized with respect to $\omega_{norm} = T_{i0}/(eB_0a^2) = 2.5\,10^4 s^{-1}$. Results obtained with the numerical method in configuration space are represented with circles, results computed with the Fourier approach with and without considering GC drifts are plotted with stars and crosses respectively. The solution to the local dispersion relation (19) parameterized with respect to the radial variable s, is drawn with a dashed line. An oval-shaped path defined by the conformal transformation (42) of the unitary disc with $\tilde{\omega}\,/\omega_{norm} = -2.1 + 1.3\,i$, $r/\omega_{norm} = 1.2$, $E = 0.1$, allowing one to localize simultaneously the three most unstable modes, appears in full line. Neglecting the GC drifts is indeed a good approximation, however their effect is always destabilizing as the magnetic curvature in a cylindrical geometry is everywhere unfavorable. The radial computation domain is taken $0.4 < s < 0.7$, so as to be centered on the mode rational surface $s_0 = 0.548$ $(q_s(s_0) = m/n)$. When solving in configuration space, typically $n_r = 100$ finite elements are needed and

$n_\nu = 50$ points for the ν integrations appearing in the coupling elements, to obtain good convergence (accuracy of $\sim 1\%$) of the most unstable mode. Fig.2 shows the convergence of the growth rate of the most unstable mode. Fig.3 a) depicts the corresponding mode computed in radial Fourier space, Fig.3 b) the same field transformed to configuration space and Fig.3 c) the poloidal structure. When solving in Fourier space, equilibrium is sampled with typically $n_r = 64$ points and the perturbation is represented with $2k_{max} + 1 = 121$ radial Fourier components. Considering GC drifts, the velocity integrals were performed using 10-20 points per thermal velocity. When approaching marginal stability the number of points must be increased so as to integrate correctly the resonant denominator.

In Fig.4 the mode numbers (m, n) are increased proportionally so as to hold the ratio $m/n = 1.6$ unchanged and the mode localized around the same rational surface. Fig.4 a) shows the normalized frequency and growth rate as a function of m. The perpendicular wave number normalized with respect to the ion Larmor radius is averaged over the eigenmode of the most unstable mode and plotted in Fig.4 b). The growth rate peaks as $< k_\perp \lambda_L >$ goes through 1, typical for slab-ITG instabilities. The root mean squared width, normalized with respect to λ_L, is given in Fig.4 c). Similar scans were repeated for two other rational surfaces $s_0 = 0.316$ $(m/n = 1.2)$ and $s_0 = 0.707$ $(m/n = 2.0)$. The growth rates of the most unstable modes are plotted in Fig.5 a) and the diffusion coefficient based on the mixing length etimate [22] in Fig.5 b). All these values were computed in configuration space and checked by the Fourier space method.

V. CONCLUSIONS

When solving the linearized gyrokinetic problem in a curved system, a wave decomposition into basic modes compatible with the magnetic surfaces turns out to be more practical then the commonly used plane wave decomposition. The difficulties arising with such a representation on the magnetic axis are negligible for a linear study. Numerical methods for inverting the final integral equation in configuration and Fourier space have been presented. The second approach is advantageous in many respects, even when considering realistic equilibrium profiles. An elaborated Niquist technique proves to be efficient for localizing the unstable spectrum in the complex frequency plane. In a following publication we shall present how these methods have been applied successfully to a true toroidal system.

ACKNOWLEDGMENT

This work was partly supported by the Swiss National Science Foundation.

APPENDIX

We summarize here the derivation leading to the eigenvalue equation in the case of plane wave decomposition.

The decomposition in plane waves in the poloidal plane for a perturbation of the form (9) is given by

$$\begin{aligned}\hat{\phi}\,(\vec{k}_\perp) &= \frac{1}{(2\pi)^2}\int d\,\vec{r}\;\phi(\vec{r})e^{-i\vec{k}_\perp\cdot\vec{r}} \\ &= \frac{1}{(2\pi)^2}\int_0^{+\infty}\rho d\rho\phi(\rho)\int_0^{2\pi}d\theta\exp i(m\theta - k_\perp\rho\cos(\theta-\alpha)) \\ &= (-i)^m\frac{e^{im\alpha}}{2\pi}\int_0^{+\infty}\rho d\rho\phi(\rho)J_m(k_\perp\rho), \end{aligned} \tag{43}$$

where $(k_\perp,\alpha)$ are the polar coordinates of the poloidal component $\vec{k}_\perp$ of the plane wave vector $\vec{k}$. Inserting this relation in Eq.(7) and carrying out the equivalent steps as for the cylindrical wave decomposition leads to the following eigenvalue equation:

$$-\varrho_q^{int}(\rho) = \int \rho' d\rho' \mathcal{K}(\rho, \rho'; \omega)\phi(\rho') = \varrho_q^{ext}(\rho), \tag{44}$$

$$\mathcal{K}(\rho, \rho'; \omega) = \frac{Ne^2}{T_i}\left[\frac{1}{\rho}\left(\frac{1}{\tau}+1\right)\delta(\rho-\rho') - \mathcal{N}(\rho, \rho'; \omega)\right], \tag{45}$$

$$\begin{aligned}\mathcal{N}(\rho, \rho'; \omega) &= \left(\frac{\omega^\star}{\omega}-1\right)(W-1)\int_0^{+\infty} k_\perp dk_\perp J_m(k_\perp\rho)J_m(k_\perp\rho')\Lambda_0(\xi) \\ &= \left(\frac{\omega^\star}{\omega}-1\right)(W-1)\frac{1}{2\pi\lambda_L^2}\int_0^\pi \frac{d\nu}{(1-\cos\nu)} \times \\ &\quad \Lambda_m\left(\frac{\rho\rho'}{2\lambda_L^2(1-\cos\nu)}\right)\exp-\left[\left(\frac{\rho-\rho'}{2\lambda_L}\right)^2\frac{1}{1-\cos\nu}\right].\end{aligned} \tag{46}$$

REFERENCES

[1] J.W.Connor, R.J.Hastie, and J.B.Taylor, Phys.Rev.Lett. **40**, 396 (1978)

[2] E.A.Frieman, G.Rewoldt, W.M.Tang, and A.H.Glasser, Phys.Fluids **23**, 1750 (1980)

[3] G.Rewoldt, W.M.Tang, and M.S.Chance, Phys.Fluids **25**, 480 (1982)

[4] X.Garbet, L.Laurent, F.Mourgues, J.P.Roubin, and A.Samain, J.Comp.Phys., **87**, 249 (1990)

[5] J.Q.Dong, W.Horton, and J.Y.Kim, Phys.Fluids B **4**, 1867 (1992)

[6] M.Kotschenreuther, G.Rewoldt, W.M.Tang, Comp.Phys.Comm., **88**, 128 (1995)

[7] S.E.Parker, W.W.Lee, and R.A.Santoro, Phys.Rev.Lett. **71**, 2043 (1993)

[8] M.Kotschenreuther, W.Dorland, M.A.Beer, and G.W.Hammett, Phys.Plasmas **2**, 2381 (1995)

[9] R.Marchand, W.M.Tang, G.Rewoldt, Phys.Fluids **23**, 1164 (1980)

[10] W.M.Tang, G.Rewoldt, Phys.Fluids B **5**, 2451 (1993)

[11] R.Marchand, C.F.Zhang, and Y.C.Lee, Phys.Fluids **26**, 194 (1983)

[12] R.D.Ferraro, H.Sanuki, R.G.Littlejohn, and B.D.Fried, Phys.Fluids **28**, 2181 (1985)

[13] S.Brunner, M.Fivaz, J.Vaclavik, K.Appert, T.M.Tran, in Proceedings of the Joint Varenna-Lausanne International Workshop on Theory of Fusion Plasmas, Varenna 1996, 101 (Editrice Compositori, Bologna, 1997)

[14] B.Davies, Jour.Comp.Phys., **66**, 36 (1986)

[15] P.J.Catto, Plasma Physics, **20**, 719 (1977)

[16] I.S.Gradshteyn and I.M.Ryzhik, Table of Integrals, Series, and Products (Academic, New York, 1965)

[17] B.D.Fried and S.D.Conte, The Plasma Dispersion Function (Academic, New York, 1961)

[18] O.Sauter, J.Vaclavik, and F.Skiff, Phys.Fluids B **2**, 475 (1990)

[19] A.B.Mikhailovskii, Theory of Plasma Instabilities, Volume 2: Instabilities of an Inhomogeneous Plasma (Consultants Bureau, New York, 1974)

[20] S.Brunner and J.Vaclavik, in Proceedings of the 22nd European Physical Society Conference on Controlled Fusion and Plasma Physics, Bournemouth 1995, IV-241 (European Physical Society, Abingdon, 1995)

[21] W.Gautschi, SIAM J.Numer.Anal., **7**, 187 (1970)

[22] B.B.Kadomtsev, Plasma Turbulence (Academic, London and New York, 1965)

Figure Captions

FIG. 1. Spectrum in complex frequency plane of highest growing global modes ($m = 8, n = 5$). Circles are results obtained solving in configuration space, stars and crosses were computed in Fourier space with and without considering GC drifts respectively. A typical path for sampling the determinant of the system is drawn in full line. The solution to the local dispersion relation parameterized by the radial variable s is plotted with a dashed line.

FIG. 2. Convergence of growth rate for the most unstable mode ($m = 8, n = 5$) versus $1/n_r^2$ obtained by the method in configuration space.

FIG. 3. a) Radial Fourier representation of the most unstable mode (m=8, n=5). b) The same field transformed to configuration space. Full and dashed lines are respectively real and imaginary part. c) Corresponding poloidal structure. These results were obtained using the method in Fourier space.

FIG. 4. a) Normalized frequency and growth rate of the most unstable mode with respect to m holding $m/n = 1.6$ fixed. b) Average value of $k_\perp \lambda_L$. c) Radial width normalized to λ_L. These results were obtained with the method in configuration space and checked with the Fourier approach.

FIG. 5. a) Growth rate of the most unstable mode with respect to m holding successively $m/n = 1.2, 1.6, 2.0$ fixed. b) Corresponding mixing length estimate $D_{ML} = \gamma/k_\perp^2$ for diffusion coefficient.

FIG.1 Brunner

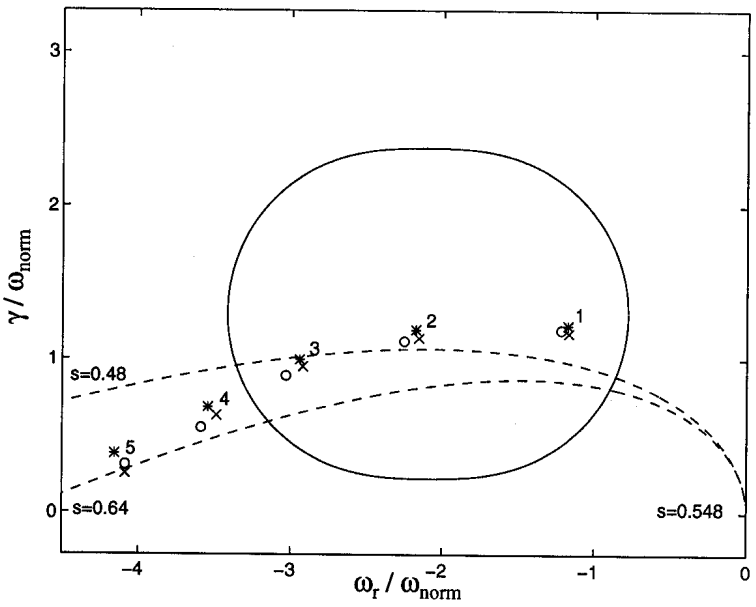

FIG.2 Brunner

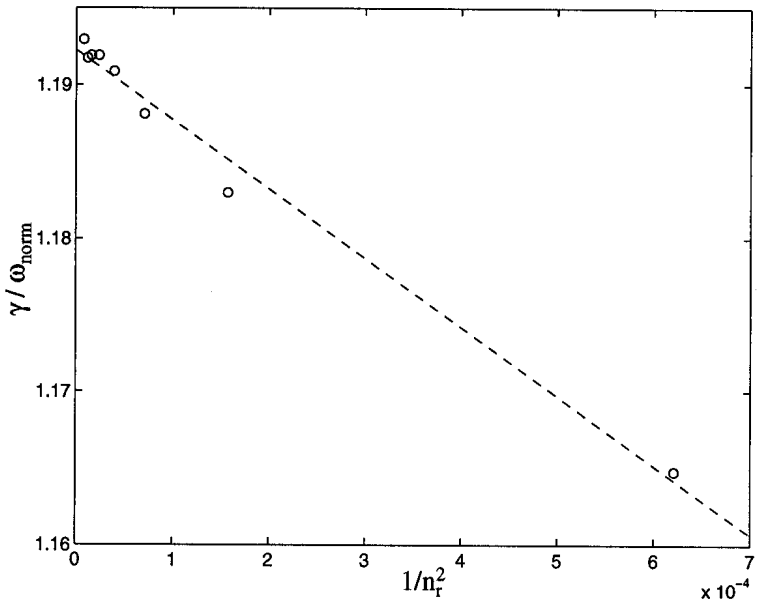

FIG.3 a), b), c) Brunner

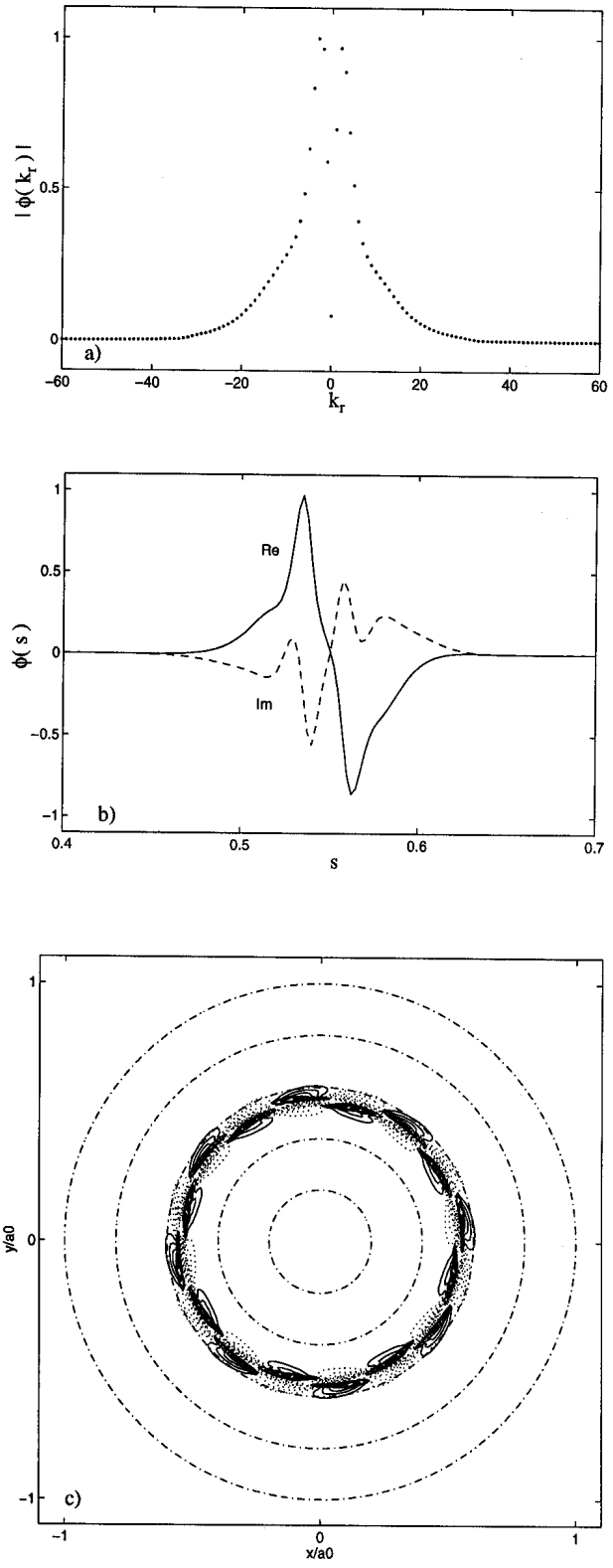

FIG.4 a), b), c) Brunner

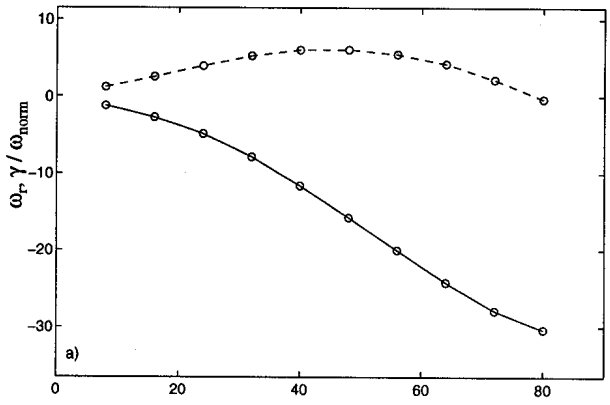

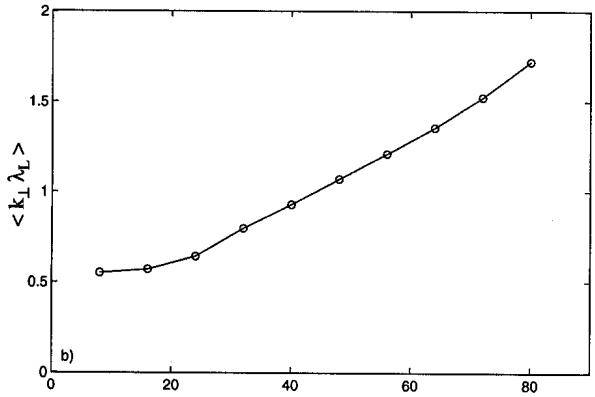

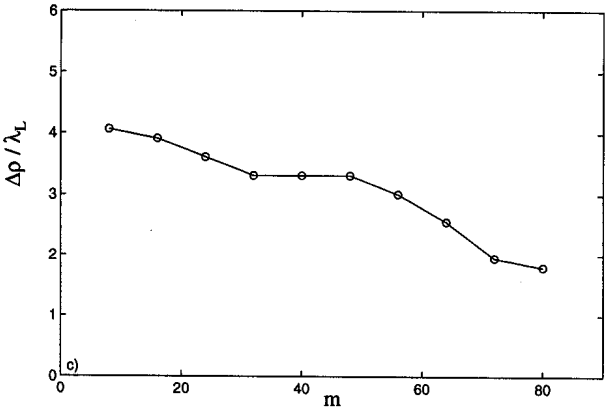

FIG.5 a), b) Brunner